

# Magnetic Compton profiles of Fe and Ni corrected by dynamical electron correlations

D. Benea<sup>a</sup>, J. Minár<sup>b</sup>, S. Mankovsky<sup>b</sup>, L. Chioncel<sup>c,d</sup> and H. Ebert<sup>b</sup>

<sup>a</sup>Faculty of Physics, Babes-Bolyai University, Kogalniceanu Str. 1, Ro-400084 Cluj-Napoca, Romania

<sup>b</sup>Chemistry Department, University Munich, Butenandstr. 5-13, D-81377 München, Germany

<sup>c</sup>Augsburg Center for Innovative Technologies, University of Augsburg, D-86135 Augsburg, Germany and

<sup>d</sup>Theoretical Physics III, Center for Electronic Correlations and Magnetism, Institute of Physics, University of Augsburg, D-86135 Augsburg, Germany

Magnetic Compton profiles (MCPs) of Ni and Fe along [111] direction have been calculated using a combined Density Functional and many-body theory approach. At the level of the local spin density approximation the theoretical MCPs does not describe correctly the experimental results around the zero momentum transfer. In this work we demonstrate that inclusion of electronic correlations as captured by Dynamical Mean Field Theory (DMFT) improves significantly the agreement between the theoretical and the experimental MCPs. In particular, an energy decomposition of Ni MCPs gives indication of spin polarization and intrinsic nature of Ni 6 eV satellite, a genuine many-body feature.

PACS numbers: 71.15.Mb, 71.20.Be, 75.30.-m

The magnetic Compton scattering is a well-established technique for probing the spin-dependent momentum densities of magnetic solids<sup>1,2</sup>. Compared with other experimental techniques, Compton scattering offers several advantages. Compton scattering is an inelastic process, in which an energetic photon collides with a single electron and transfers energy to it. Since the scattering is from a single-electron and (to a good approximation) occurs at a single point in space, the process must be incoherent and is supplying an average over real space. Therefore, Compton scattering is related directly to the electronic ground state, whereas other spectroscopic methods (e.g. photoemission spectroscopy) involve excited states.

In addition Compton scattering allows for a rather fundamental test of the theories used to describe the spin dependent momentum density, since these theoretical methods are tailored to give predictions for the ground state properties. Several theoretical methods have been used in the past to describe the electron momentum density and to analyze the experimental MCPs<sup>3-9</sup>. Most of the corresponding calculations were done within the local spin density approximation (LSDA) for the exchange-correlation potential. In general, the theoretical profiles obtained using LSDA show an overall agreement with the experimental measurements, except within the region  $p_z < 1$  a.u.. It was pointed out that the discrepancy between the experimental and theoretical MCP could be attributed to missing electron-electron correlations in band models<sup>10</sup>. Along this line, recently, several theoretical methods beyond LSDA have been applied in order to describe the features of the MCP which cannot be explained using the LSDA-based approach and to improve the agreement with experiment<sup>8,11,12</sup>. The LSDA + U method has been applied by Tokii et al.<sup>8</sup> to calculate the MCPs of Fe, showing improvement for [100] and [110] directions but still underestimates near the origin the MCP for [111] direction. Also, one should mention the calculations of the Ni MCP done by Kubo<sup>11</sup> implemented within

the GW scheme based on the FLAPW method. His calculations are in overall agreement with experiment, but still remarkable discrepancies are found for the Ni [110] and [111] MCP spectra.

The electronic structure of fcc Ni has been subject of intensive studies as a prototype of itinerant electron ferromagnets, since they indicate a failure of the one-electron theory<sup>13-16</sup>. The LSDA calculations for fcc Ni cannot reproduce some features of the electronic structure of Ni observed experimentally. The valence band photoemission spectra of Ni<sup>17,18</sup> shows a 3d-band width that is about 30 % narrower than obtained from the LSDA calculations<sup>15</sup>. Second, the spectra show a dispersionless feature at about 6 eV binding energy (the so-called 6 eV satellite)<sup>19,20</sup>, which again cannot be reproduced by the LSDA calculations. Third, the magnetic exchange-splitting is overestimated by LSDA calculations<sup>15</sup> compared with the experimental data<sup>21</sup>. On the other hand, an improved description of correlation effects for the 3d electrons via the LSDA+DMFT<sup>22-25</sup> gives the width of the occupied 3d bands of Ni properly and reproduce the exchange splitting and the 6 eV satellite structure in the valence band.

In view of these LSDA+DMFT improvements<sup>22,23</sup> upon the magnetic properties of Fe and Ni, the comparison of experimental MCP with the LSDA+DMFT theory provides some new information besides offering a test for the impact of electronic correlations. In particular we demonstrate here that the LSDA+DMFT calculations improves also the agreement between theory and experiment for Fe and Ni MCPs. In the following we briefly discuss the theoretical approach and present the calculated MCPs of Fe and Ni together with the experimental data. Finally, the LSDA and LSDA+DMFT calculated MCPs of Ni have been decomposed and the contribution of different energy windows in the valence band have been compared in order to extract the features of electron correlations and to show their energy-dependency. Such a decomposition provides the evidence of the connection

between the MCP contribution in the lower part of the valence band and the existence of 6 eV satellite, both features being captured only within LSDA+DMFT.

The calculations were done using the spin-polarized relativistic Korringa-Kohn-Rostoker (SPR-KKR) method in the atomic sphere approximation (ASA)<sup>26</sup>. The computational scheme is based on the KKR Green function formalism, which makes use of multiple scattering theory, and was recently extended to compute MCPs<sup>27-29</sup>. The spin projected momentum density  $n_{m_s}(\vec{p})$  (where  $m_s = \uparrow (\downarrow)$ ) is computed using the LSDA(+DMFT) Green's functions in momentum space as

$$n_{m_s}(\vec{p}) = -\frac{1}{\pi} \int_{-\infty}^{E_F} \Im G_{m_s}^{LSDA(+DMFT)}(\vec{p}, \vec{p}, E) dE.$$

In order to analyze the momentum density and the corresponding MCPs in different energy ranges, we use a decomposition of the above formula in the form:

$$n_{m_s, \Delta E}(\vec{p}) = -\frac{1}{\pi} \int_{E_1}^{E_2} \Im G_{m_s}^{LSDA(+DMFT)}(\vec{p}, \vec{p}, E) dE,$$

where  $\Delta E = E_2 - E_1$  represent the width of the energy window. The MCP seen in each energy window  $\Delta E$  is obtained by performing a double integral in the momentum plane perpendicular to the scattering momentum  $\vec{p}_z$

$$J_{mag}^{LSDA(+DMFT)}(p_z) = \int \int (n_{\uparrow}(\vec{p}) - n_{\downarrow}(\vec{p})) dp_x dp_y.$$

Here the electron momentum density for a given spin orientation is given by  $n_{\uparrow(\downarrow)}(\vec{p})$ . The area under the MCP is equal to the spin moment per Wigner-Seitz cell:  $\int_{-\infty}^{+\infty} J_{mag}^{LSDA(+DMFT)}(p_z) dp_z = \mu_{spin}^{LSDA(+DMFT)}$ . In the actual calculations the experimental lattice parameters of Fe and Ni have been used ( $a_{Fe/Ni} = 0.287/0.352$  nm). The exchange-correlation potentials parameterized by Vosko, Wilk and Nusair<sup>30</sup> were used for the LSDA calculations. For integration over the Brillouin zone the special points method has been used<sup>31</sup>. In addition to the LSDA calculations, a charge and self-energy self-consistent scheme for correlated systems based on the KKR approach with the many body effects described by the means of dynamical mean field theory (DMFT) has been applied<sup>23</sup>. As a DMFT solver the relativistic version of the so-called Spin-Polarized T-Matrix Fluctuation Exchange approximation<sup>32,33</sup> was used. The realistic multi-orbital interaction has been parameterized by the average screened Coulomb interaction  $U$  and the Hund exchange interaction  $J$ . The  $J$  parameter can be calculated directly within the LSDA and is approximately the same for all 3d elements. The parameter  $U$  is strongly affected by the metallic screening and it is estimated for the 3d metals to lie between 1 and 3 eV. In the present calculations we used  $J = 0.9$  eV and  $U = 2.3$  eV.

The MCPs of Ni [111] calculated on the basis of the LSDA and LSDA+DMFT, respectively, are shown in

Fig. 1, together with the experimental data. The Gaussian broadening applied to the calculated MCPs corresponds to the experimental resolution. The experimental MCPs stemming from Dixon et al.<sup>7</sup> have been normalized to the experimentally determined spin moment ( $0.56 \mu_B$ ). After broadening, the calculated KKR MCP spectra have been normalized to the calculated spin moment ( $0.6 \mu_B$  by LSDA and LSDA+DMFT). As can be seen, in the high-momentum region ( $p_z \geq 2$  a.u.) the correlation effects have a small influence on the magnetic spin density. In the momentum region  $0 \leq p_z \leq 2$  a.u., taking into account the electron correlations by LSDA+DMFT approach improves the agreement with the experimental spectra considerably. Our LSDA+DMFT calculations can reproduce the dip in the [111] profile at  $\sim 0.8$  a.u., which was clearly underestimated by the LSDA calculations.

The LSDA and LSDA+DMFT calculated MCPs of Fe [111] are shown in Fig. 2 together with the experimental spectra of McCarthy et al.<sup>34</sup>. The experimental MCP has been normalized to a spin momentum of  $2.07 \mu_B$ . The calculated spectra have been convoluted with a Gaussian of 0.42 a.u., corresponding to the experimental resolution. After convolution, the calculated MCPs have been scaled at a spin momentum of  $2.3 \mu_B$  (the LSDA calculated MCP) and  $2.19 \mu_B$  (the LSDA+DMFT calculated MCP), respectively. Although both calculated MCPs show agreement with the experiment in the high momentum region, the shoulder at  $\sim 0.5$  a.u. is diminished in the LSDA+DMFT calculated MCP, improving the agreement with the experimental spectra also in the low momentum region.

The theoretical MCP of Ni [111] has been decomposed into contributions from different energy windows. To illustrate the decomposition into energy windows, the LSDA calculated MCP stemming from the energy bands

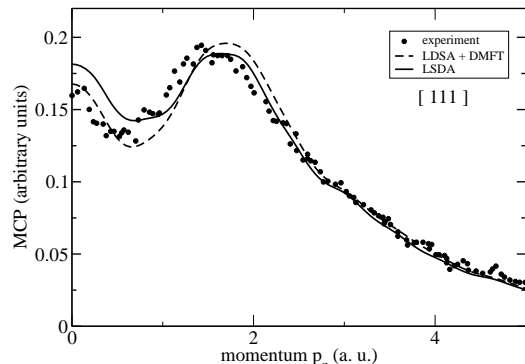


FIG. 1: MCPs of Ni [111] calculated via the KKR method within the LSDA and LSDA+DMFT approach. The theoretical curves have been convoluted with a Gaussian of 0.43 a.u. FWHM, corresponding to the experimental resolution. The experimental data stem from Dixon et al.<sup>7</sup>.

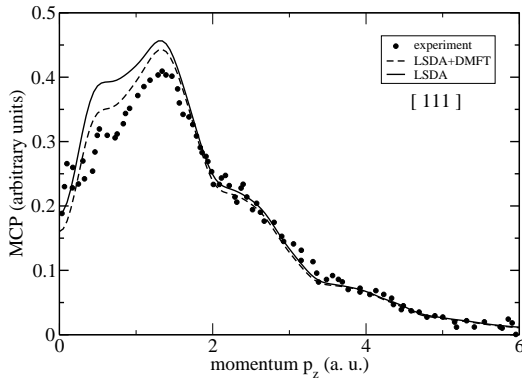


FIG. 2: MCPs of Fe [111] calculated via the KKR method within the LSDA and LSDA+DMFT approach. The theoretical curves have been convoluted with a Gaussian of 0.42 a.u. FWHM, corresponding to the experimental resolution. The experimental data stem from McCarthy et al.<sup>34</sup>.

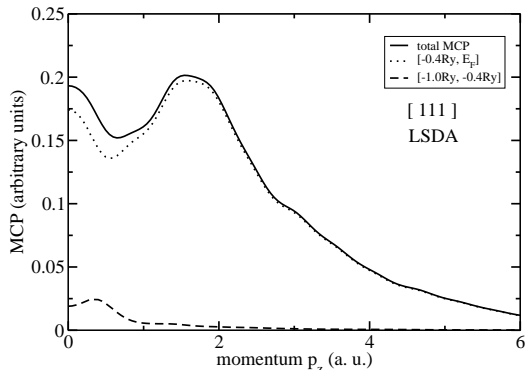


FIG. 3: The theoretical MCPs of Ni [111] obtained from LSDA calculations. The MCPs have been decomposed into contributions of two energy windows:  $[-1.0 \text{ Ry}, -0.4 \text{ Ry}]$  and  $[-0.4 \text{ Ry}, E_F]$ .

below the Fermi level in the range  $[-0.4 \text{ Ry}, E_F]$  and  $[-1.0 \text{ Ry}, -0.4 \text{ Ry}]$  are shown in Fig. 3. As can be seen, the main contribution of the LSDA calculated MCP is stemming from the energy bands situated between  $-0.4 \text{ Ry}$  and the Fermi level. The bands at energy lower than  $-0.4 \text{ Ry}$  have just a small positive contribution to the MCP within the momentum range  $p_z \leq 1 \text{ a.u.}$ . The corresponding decomposition has been performed as well for the LSDA+DMFT calculated MCP and the results are shown in Fig. 4. The contribution of the energy bands situated between  $-0.4 \text{ Ry}$  and Fermi level has an important negative polarization for  $p_z \leq 1 \text{ a.u.}$ . According to the s, p and d-electron decomposition (not shown here) the negative contribution stem from s and p electrons. The overall negative polarization of s and p electrons is increased in the LSDA+DMFT MCP

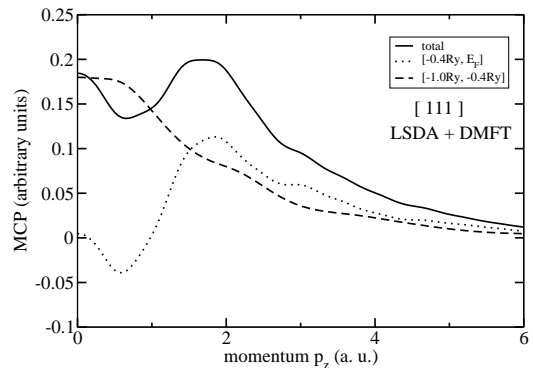


FIG. 4: The theoretical MCP of Ni [111] obtained from KKR LSDA+DMFT calculations. The MCPs have been decomposed into contributions of two energy windows:  $[-1.0 \text{ Ry}, -0.4 \text{ Ry}]$  and  $[-0.4 \text{ Ry}, E_F]$ .

compared with the LSDA approach.

An essential feature is the important positive contribution of the electronic states in the energy window  $[-1.0 \text{ Ry}, -0.4 \text{ Ry}]$  to the MCP, that is similar for different scattering directions. The MCP carries information about all spin-polarized electrons in the system and about their localization. A broad contribution in the MCP is an indication for dominating localized spin states<sup>1</sup>. As the LSDA+DMFT MCPs are broader than the LSDA ones we have a clear indication that the spin magnetic densities have the tendency to localize in the presence of the electronic correlations. As this MCP broadening is seen in the energy range  $[-1.0 \text{ Ry}, -0.4 \text{ Ry}]$  where the well known feature of the correlated electronic bands of Ni, namely the 6 eV satellite (0.44 Ry) is situated, a direct connection between this two correlation features is presumable. As was shown by earlier calculations<sup>22</sup> and was confirmed by photoemission experiments<sup>35</sup>, the 6 eV satellite is spin polarized and accordingly has to be connected with the MCP. The general interpretation of the 6 eV satellite relates this feature to an excited state involving two 3d holes bound on the same Ni site, therefore it is not accessible to any LSDA calculations. On contrary the LSDA+DMFT approach is able to capture such processes via the explicit existence within the interacting Hamiltonian of the four index form of the Coulomb matrix. Although the correlation induced satellite is absent in Fe, the proper description of the angle-resolved photoemission spectra cannot be done by LSDA but by LSDA+DMFT<sup>36</sup>. In the case of Fe, a broad contribution of the LSDA+DMFT MCP is also obtained in the energy range  $[-1.0 \text{ Ry}, -0.4 \text{ Ry}]$  and consequently a similar tendency of localization of the spin density is expected.

In conclusion, the MCPs of Fe and Ni have been determined using the SPR-KKR band structure method within the LSDA and LSDA+DMFT approach, respectively. The influence of electron correlations on the MCP of Fe and Ni [111] has been discussed. For

high transfer momenta ( $(p_z \geq 2 \text{ a.u.})$ ) no significant corrections due to dynamical electronic correlations is seen in the Compton profile, therefore the dynamics of the process can be captured equally well by a LSDA approach. On contrary for small momentum transfer, a clear evidence for the interplay between the energy transferred to electron and the electronic correlations is seen: including the local but dynamical self-energy leads to an improved MCP spectra. In addition the decomposition of the Ni [111] MCPs shows a large and broad contribution by DMFT+LSDA approach stemming from the energy window between the bottom of the valence band and 0.4 Ry binding energy. For the

corresponding MCP decomposition the LSDA approach shows just a small and narrow contribution stemming from the same energy range. We consider this feature as a consequence of the localization tendency of the spin density due to electronic correlations.

DB acknowledge the financial support of the Deutsches Forschungsgemeinschaft through FOR 1346 and the project POSDRU 89/1.5/S/60189 with the title 'Post-doctoral Programs for sustainable Development in a Knowledge Based Society'. Financial support by the Bundesministerium für Bildung und Forschung (05K10WMA) is also gratefully acknowledged.

- 
- <sup>1</sup> M. J. Cooper, Rep. Prog. Phys. **48**, 415 (1985).  
<sup>2</sup> S. W. Lovesey and S. P. Collins, *X-Ray Scattering and Absorption by Magnetic Materials* (Clarendon Press Oxford, 1996), chap. 7.  
<sup>3</sup> S. Wakoh and Y. Kubo, J. Magn. Magn. Materials **5**, 202 (1977).  
<sup>4</sup> Y. Kubo and S. Asano, Phys. Rev. B **42**, 4431 (1990).  
<sup>5</sup> Y. Tanaka, N. Sakai, Y. Kubo, and H. Kawata, Phys. Rev. Letters **70**, 1537 (1993).  
<sup>6</sup> T. Baruah, R. R. Zope, and A. Kshirsagar, Phys. Rev. B **62**, 16435 (2000).  
<sup>7</sup> M. A. G. Dixon, J. A. Duffy, S. Gardelis, J. E. McCarthy, M. J. Cooper, S. B. Dugdale, T. Jarlborg, and D. N. Timms, J. Phys.: Condensed Matter **10**, 2759 (1998).  
<sup>8</sup> M. Tokii and M. Matsumoto, J. Phys.: Condensed Matter **18**, 3639 (2006).  
<sup>9</sup> Z. Major, S. B. Dugdale, R. J. Watts, J. Laverock, J. J. Kelly, D. C. R. Hedley, and M. A. Alam, J. Phys. Chem. Solids **65**, 2011 (2004).  
<sup>10</sup> G. E. W. Bauer and J. R. Schneider, Phys. Rev. B **31**, 681 (1985).  
<sup>11</sup> Y. Kubo, J. Phys. Chem. Solids **65**, 2077 (2004).  
<sup>12</sup> Y. Sakurai, A. Deb, M. Itou, A. Koizumi, Y. Tomioka, and Y. Tokura, J. Phys.: Condensed Matter **16**, S5717 (2004).  
<sup>13</sup> A. Liebsch, Phys. Rev. Letters **43**, 1431 (1979).  
<sup>14</sup> A. Liebsch, Phys. Rev. B **23**, 5203 (1981).  
<sup>15</sup> C. S. Wand and J. Callaway, Phys. Rev. B **15**, 298 (1977).  
<sup>16</sup> W. Eberhardt and E. W. Plummer, Phys. Rev. B **21**, 3245 (1980).  
<sup>17</sup> D. E. Eastman, F. J. Himpsel, and J. A. Knapp, Phys. Rev. Letters **40**, 1514 (1978).  
<sup>18</sup> F. J. Himpsel, J. A. Knapp, and D. E. Eastman, Phys. Rev. B **19**, 2919 (1979).  
<sup>19</sup> S. Hüfner and G. K. Wertheim, Phys. Letters **51A**, 299 (1975).  
<sup>20</sup> C. Guillot, Y. Ballu, J. Paigné, J. Lecante, K. P. Jain, P. Thiry, R. Pinchaux, Y. Petroff, and L. M. Falicov, Phys. Rev. Letters **39**, 1632 (1977).  
<sup>21</sup> E. Dietz, U. Gerhardt, and C. J. Maetz, Phys. Rev. Letters **40**, 892 (1978).  
<sup>22</sup> A. I. Lichtenstein, M. I. Katsnelson, and G. Kotliar, Phys. Rev. Letters **87**, 067205 (2001).  
<sup>23</sup> J. Minár, L. Chioncel, A. Perlov, H. Ebert, M. I. Katsnelson, and A. I. Lichtenstein, Phys. Rev. B **72**, 045125 (2005).  
<sup>24</sup> J. Braun, J. Minár, H. Ebert, M. I. Katsnelson, and A. I. Lichtenstein, Phys. Rev. Letters **97**, 227601 (2006).  
<sup>25</sup> J. Minár, J. Phys.: Condensed Matter **23**, 253201 (2011).  
<sup>26</sup> H. Ebert, D. Ködderitzsch, and Minár, Rep. Prog. Phys. **74**, 096501 (2011).  
<sup>27</sup> Z. Szotek, B. L. Gyorffy, G. M. Stocks, and W. M. Temmerman, J. Phys. F: Met. Phys. **14**, 2571 (1984).  
<sup>28</sup> D. Benea, S. Mankovsky, and H. Ebert, Phys. Rev. B **73**, 094411 (2006).  
<sup>29</sup> D. Benea, Ph.D. thesis, LMU München (2004).  
<sup>30</sup> S. H. Vosko, L. Wilk, and M. Nusair, Can. J. Phys. **58**, 1200 (1980).  
<sup>31</sup> H. J. Monkhorst and J. D. Pack, Phys. Rev. B **13**, 5188 (1976).  
<sup>32</sup> M. I. Katsnelson and A. I. Lichtenstein, Eur. Phys. J. B **30**, 9 (2002).  
<sup>33</sup> L. V. Pourovskii, M. I. Katsnelson, and A. I. Lichtenstein, Phys. Rev. B **72**, 115106 (2005).  
<sup>34</sup> J. E. McCarthy, M. J. Cooper, P. K. Timms, A. Brahmia, D. Laundry, P. P. Kane, G. Clark, and D. Laundry, J. Synchr. Rad. **4**, 102 (1997).  
<sup>35</sup> K. N. Altmann, D. Y. Petrovykh, G. J. Mankey, N. Shannon, N. Gilman, M. Hochstrasser, R. F. Willis, and F. J. Himpsel, Phys. Rev. B **61**, 15661 (2000).  
<sup>36</sup> J. Sanchez-Barriga, J. Fink, V. Boni, I. Di Marco, J. Braun, J. Minár, A. Varykhalov, O. Rader, V. Bellini, F. Manghi, H. Ebert, M. I. Katsnelson, A. I. Lichtenstein, O. Eriksson, W. Eberhardt, and H. A. Dürr, Phys. Rev. Lett. **103**, 267203 (2009).